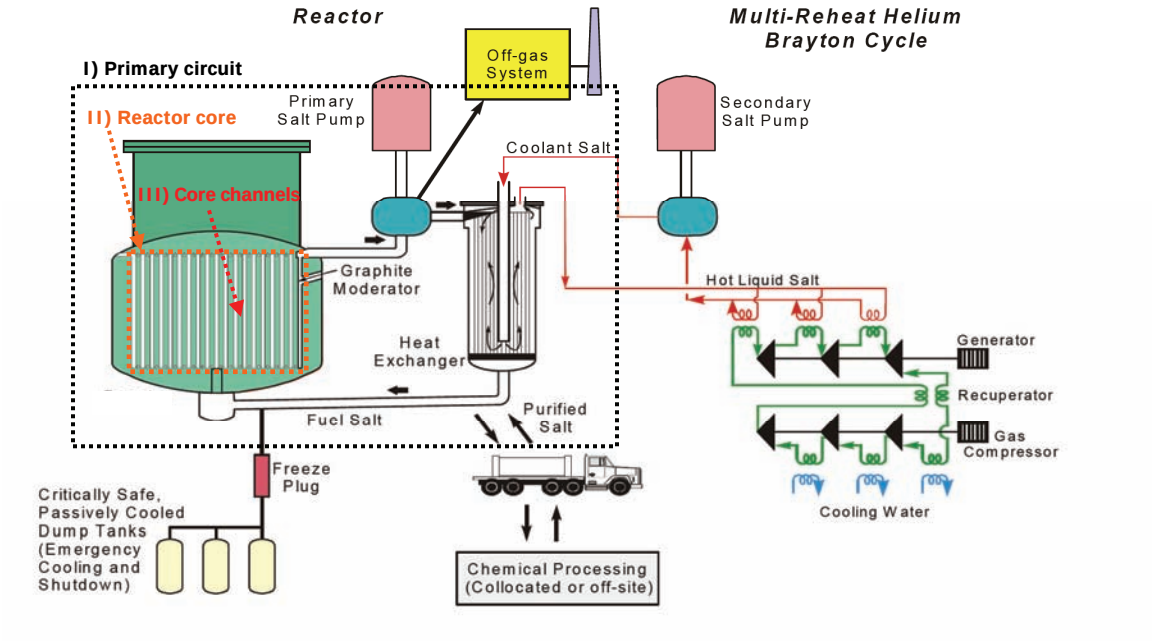

Figure 1. Typical layout of a nuclear power plant based on thermal (graphite moderated) MSR technology (from Ref. [1]): I) primary circuit; II) reactor core; III) core channels.

2. Multi-physics model

The multi-physics modelling adopted in this work consists of eight coupled partial differential equations describing the fluid motion (RANS – Reynolds Averaged Navier-Stokes equations with the standard k-ε turbulence model), the energy balance, the neutron and the precursors balances (see Appendices A and B).

Two different 2-D geometries have been considered for the analyses, i.e.: a Cartesian (x,y) geometry (0.58 m x 3.46 m rectangular box) representing a finite region of a sub-critical reactor (case a, as in Ref. [8]); an axial symmetric cylindrical geometry (r,z) representing a MSR (sub-critical) core channel (case b, shown in Figure 2). The channel considered in the present work is featured by an inner and outer graphite radius of 0.29 m and 0.43 m, respectively, and a height of 3.46 m. It is worth noting that the size of the channel, in which the molten salt circulates, is a key design issue for MSRs, influencing relevant parameters like the moderating ratio, the total reactivity feedback coefficient, the breeding ratio, the graphite lifetime and the initial fissile inventory; a critical discussion of such effects, which are out of the scope of this work, can be found in [1,10,11].

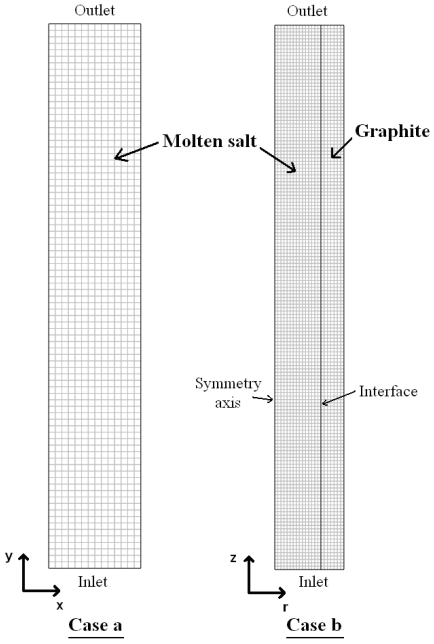

Figure 2. Geometry and mesh structure of the analyzed systems.

2.1 System of equations

The flow of the molten salt fuel is determined by the combined action of natural convection and external pumps.

The formulation adopted to evaluate the fluid motion is given in Appendix B by Eqs. (1), (2), (3), (4) and (iv), considering the buoyancy effect by means of the Boussinesq approximation – see Eqs. (i), (ii) and (iii).

The energy balance considers the convection of energy by means of the fluid motion (only for the molten salt), heat conduction, and the heat source from the nuclear reactions, as formulated in Eqs. (5), (6), (v) and (vi). It must be pointed out that the relationship between the heat sources within molten salt (S_f) and graphite (S_g) has been neglected, assuming in the graphite a uniform heat source equal to 3% of the maximum value achieved within the fuel [12]. Moreover, to a first approximation, all the heat can be considered as "prompt" (i.e., neglecting the delay of the subsequent heat generated by radioactive decay).

A neutron diffusion model, which considers one energy group and one family of precursors, is adopted, as expressed by Eqs. (7) and (8), and it is applied only within the fluid fuel region. The term S_n in Eq. (7) represents the external neutron source of the sub-critical reactor and its expression is given in [8].

The concentration of precursors can be properly described by means of Eq. (8), in which the effect of the mobility of the fluid fuel is considered, but the precursors diffusion coefficient D_c has been neglected in the simulations.

2.2 Boundary and initial conditions

The boundary conditions are chosen to be as realistic as possible within the scope of this work. For what concerns the boundary conditions for the "case a", reference is made to our previous work [8]. The boundary conditions for the "case b" have been chosen in order to simulate the behaviour of a typical MSR core channel, and axial-symmetric conditions are imposed at the channel centre (symmetry axis).

The neutron flux is assumed to vanish on boundaries. Symmetric conditions for the precursors concentration are supposed on the vertical boundaries, while a convective flux condition is applied on the outlet boundary of the fuel. On the inlet boundary, the entry concentration is assumed equal to zero, considering that the circulation time of the fuel salt out of the reactor core is much greater than the radioactive decay of precursors.

As far as the temperature is concerned, inlet boundaries stay at a prescribed temperature T_0, while convective flux conditions are applied on the outlet of both graphite and molten salt and at the outer radius of graphite matrix. At the interface between molten salt and graphite, the heat exchange is modelled by means of the *thermal wall functions* [13]. The fluid-dynamics boundary conditions are the following: the inlet velocity is assigned at the inlet boundary, the pressure is null at the outlet boundary and *logarithmic wall functions* are applied at the interface (for a detailed discussion, see Ref. [9]).

3. Simulations

The governing equations above described have been implemented in COMSOL® 3.4 using the following application modes [13]: *k-ε turbulence model* for the fluid motion; *Convection and Conduction* for the energy balance both in the fuel and the graphite; *Convection and Diffusion* for the precursors balance; *PDE General Form* for the implementation of the neutron balance equation.

The main reference data and material properties adopted in the simulations for the molten salt [6] and the graphite [14] are representative of the actual values encountered in Molten Salt Reactors without being specific to any case (see Appendix C).

The initial state assumes the reactor to be at zero power, with an established hydrodynamic pattern. A start-up transient has been simulated, adopting for the external neutron source a cosine spatial shape [6,8].

The physics of the system brings to an attainment of a steady state by relaxing the initial conditions; the evolution equations are solved as a time dependent problem by means of a transitory analysis.

Simulations have been carried out for both cases a and b in turbulent flow with a Reynolds number (Re) equal to $8 \cdot 10^4$. Moreover, for the case a, further analyses have been performed with $Re = 8 \cdot 10^5$ and compared to the simulations with laminar flow of Ref. [8], in order to evaluate the flow regime effect on the dynamic behaviour of the molten salt fuel.

4. Results and discussion

4.1 Case a

Results of the simulations are presented in Figures 3 and 4, and compared with the solution for laminar flow described in our previous work [8]. The coupling between the nuclear and the thermo-hydrodynamic models is evident, in accordance with recent literature works [6,7,8].

The comparison shown in Figure 3 points out that in laminar flow the buoyancy effect (according to the Boussinesq approximation) is more important than in the turbulent one because the fluid temperature is higher [15]. Moreover, the fluid recirculation is more evident in laminar flow; as a consequence, the precursors are more concentrated in the upper part of the domain for the turbulent case.

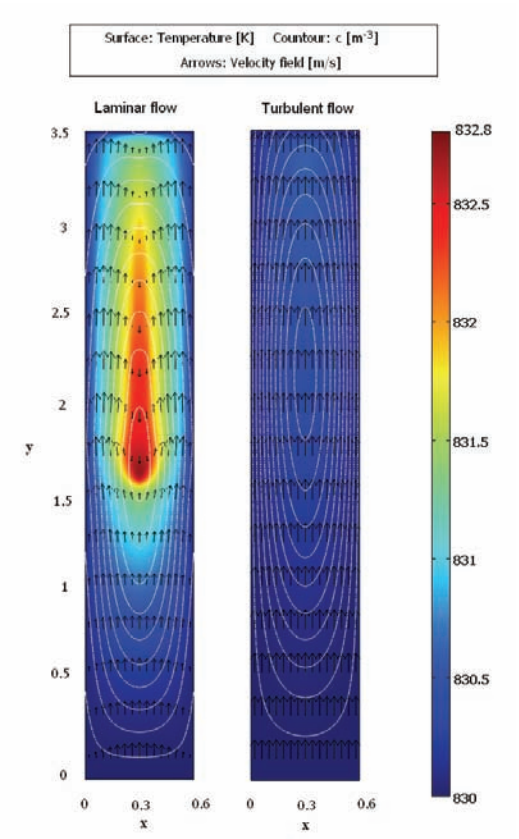

Figure 3. Case a: temperature (surface), precursors concentration (contour) and velocity field (arrows) for steady state conditions in both laminar (from Ref. [8]) and turbulent (present work, with Re = $8 \cdot 10^4$) flows.

The different flow regimes significantly influence the dynamic behaviour of the system, as shown in Figure 4: the time constant of the fluid temperature in the two considered turbulent regimes is lower than in laminar flow, showing a relevant dependence on the imposed inlet velocity, which also affects the precursors time evolution. It must be emphasized that such effect, due to the strong coupling between thermal and hydrodynamic fields, can be properly caught thanks to the adopted multi-physics approach.

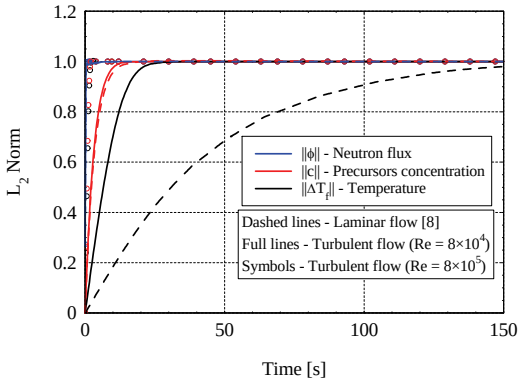

Figure 4. Case a: evolution of neutron flux ϕ, precursors concentration c, and temperature variation ($\Delta T_f = T_f - T_0$). The L_2 norm is plotted and all quantities are normalized to their final value.

4.2 Case b

Results achieved for the simulations of the start-up transient are represented in Figure 5 in terms of both the temperature profile and the velocity field. It is interesting to notice a specific feature of the graphite + molten salt (fuel/coolant) system, unlike the externally cooled solid fuel rods adopted in the conventional nuclear reactors: initially, the heat is transferred from the fuel/coolant to the graphite matrix, but a situation is eventually reached where the radial heat flux is inverted between them.

This behaviour is clear in Figure 6, where the steady state temperature profile on the channel mid-plane is also represented: after 50 s in the simulated transient, and in any case in steady state operation, the graphite temperature results higher than the molten salt temperature, due to the assumed heat transfer boundary conditions, in accordance with literature [12,14].

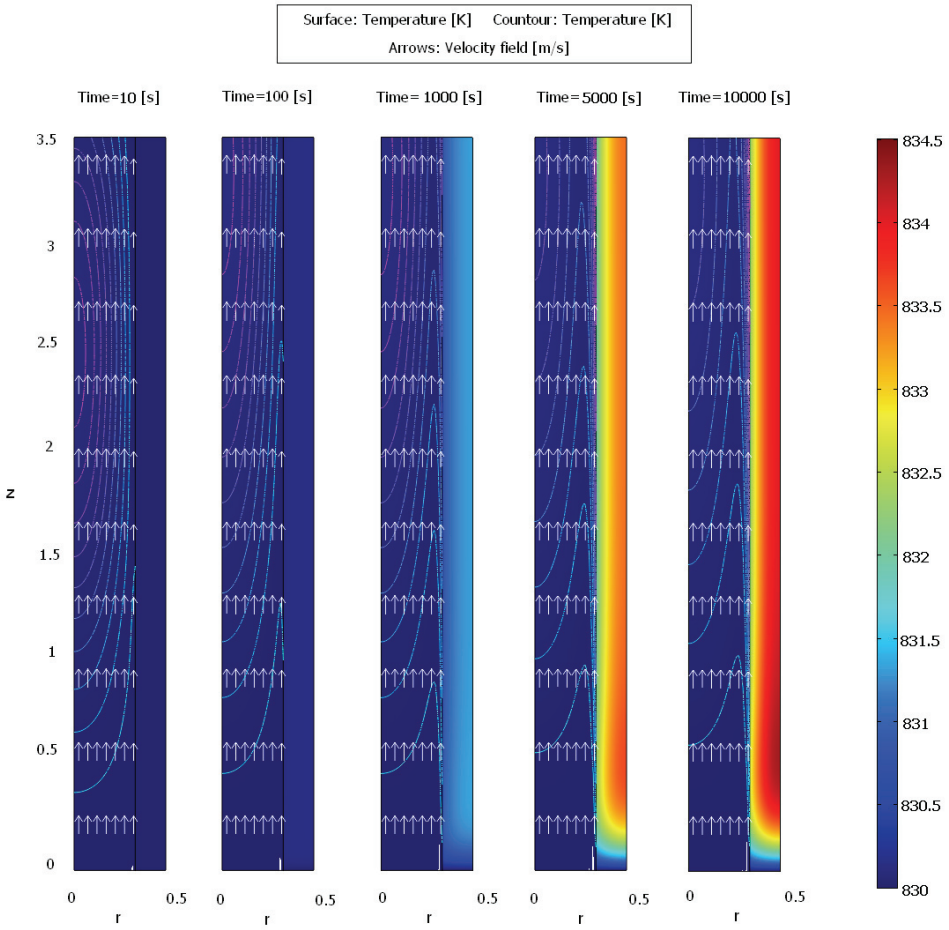

Figure 5. Case b: temperature (surface and contour) and velocity field (arrows) at different times.

The radial temperature profile of the graphite is affected by the heat transfer coefficient (h) with the molten salt: the value of the Nusselt number (Nu = 461) obtained in this case results in a very good agreement with that achievable by means of the well-known Dittus-Boelter correlation, as thoroughly discussed in [9].

The heat transfer between the graphite and the molten salt influences also their dynamic behaviour. In particular, to a first approximation, the time evolution of the graphite temperature can be described by means of the time constant τ_g given in Appendix B by Eq. (vii).

Figure 7 shows the dynamic behaviour of the system in terms of neutron flux, precursors concentration, fluid and graphite temperatures: these quantities exhibit very different time scales, which are relevant for the operation and the control of the reactor and, more in general, of the overall nuclear power conversion system, as discussed in [8].

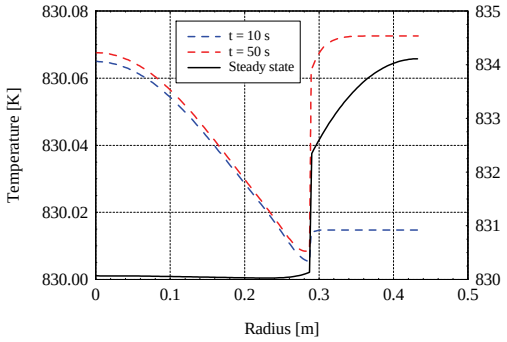

Figure 6. Case b: temperature radial profiles on the channel mid-plane at different times (dashed lines – left axis) compared to the steady state solution (full line – right axis).

Actually, four time constants can be noticed in Figure 7, which are clearly different and related to: the prompt fission neutron source (blue line, tenths of second), the delayed neutrons precursors (red line, seconds), the thermal behaviour of fluid (black line, tens of second) and the thermal behaviour of the graphite (green line, thousands of seconds). It must be noticed that the time constant of graphite is much greater than the other ones; moreover, its order of magnitude can be caught by using the simple formula given in Eq. (vii).

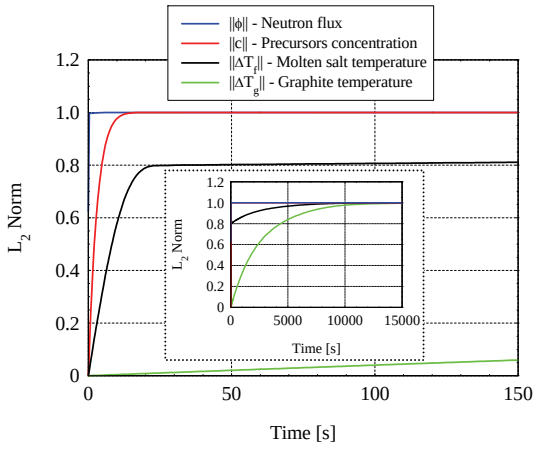

Figure 7. Case b: evolution of neutron flux ϕ, precursors concentration c, and temperature variation for both fuel (ΔT_f) and graphite ($\Delta T_g = T_g - T_0$).

As a final comment on the simulations, the adopted multi-physics approach has proved to be adequate to point out and properly evaluate the interactions between neutronic phenomena and hydrodynamics, which are specific of MSRs.

5. Conclusions

MSRs are featured by a strong coupling between neutronics and thermo-hydrodynamics, which can be properly treated by means of a multi-physics approach. In this paper a simple 2-D geometry, representing a typical channel of a sub-critical MSR that comprises both the flowing molten salt fuel and the graphite matrix, has been considered. Physics of such system can be modelled by means of eight coupled partial differential equations, describing the fluid motion and the balances of energy, neutrons and precursors. With reference to this complex and highly non linear environment, COMSOL® confirmed as an adequate tool to catch some relevant features of both the steady state and the dynamic behaviour of the considered MSR channel. Analyses have been carried out for both laminar and turbulent flow regimes, focusing on the influence that graphite has on such system. In particular, the time constants of some physical quantities have been discussed: namely, the neutron flux, the precursors concentration, the fluid and graphite temperature, whose time evolution is of extreme interest for the investigation of the dynamic behaviour as well as for of the most appropriate control strategy to be adopted in the current development of Molten Salt Reactors for Generation IV.

In short, this study has provided important information about the channel behaviour of a sub-critical MSR and paves the way for further progress concerning more complex and design-oriented simulations, which should consider more representative geometries of the power channels (if not of the whole reactor core) and more details in the neutronic modelling of both the molten salt and the graphite, as well as of their "nuclear" interaction.

6. References

1. C. Fosberg et al., Liquid Salt Applications and Molten Salt Reactors, *Proceedings of ICAPP '07*, Nice, France, May 13-18 (2007)
2. A Technology Roadmap for Generation IV Nuclear Energy Systems, issued by the U.S. DOE Nuclear Energy Research Advisory Committee and the Generation IV International Forum, GIF-002-00 (2002)
3. C. Renault, M. Delpech, Review of Molten Salt Reactor Technology, MOST Final Report, European Commission (2005)
4. M. Hron, J. Uhlìr, C. Renault, ""“Molten Salt Reactor” Current status and future prospects within European activities (MSR)", *FISA 2006 EU Research and Training in Reactor Systems*, EUR 21231, pp. 270-286 (2006)
5. A. Cammi, L. Luzzi, Expert Commentary: Innovative Techniques for the Simulation and Control of Nuclear Power Plants, in *Nuclear Energy Research Progress*, V.B. Durelle Ed., pp. 1-4. Nova Science Publishers, Hauppauge NY (2008)
6. G. Lapenta, Mathematical and Numerical Models for the Coupling of Neutronics and

Thermal-Hydrodynamics in Circulating Fuel Nuclear Reactors, in *Nuclear Reactor Physics*, pp. 195-210. CLUT, Turin (2005)
7. C. Nicolino, G. Lapenta, S. Dulla, P. Ravetto, Coupled dynamics in the physics of molten salt reactors, *Annals of Nuclear Energy*, **35**, 314-322 (2008)
8. A. Cammi, V. Di Marcello, L. Luzzi, Modelling of Circulating Nuclear Fuels with COMSOL Multiphysics, *Proceedings of the European COMSOL Conference 2007*, Grenoble, France, October 23-24, 2007, **vol. 1**, pp. 380-386 (2007)
9. V. Di Marcello, A. Cammi, L. Luzzi, Analysis of Thermal-Hydraulic Behaviour of the Molten Salt Nuclear Fuel, *Proceedings of the International Conference Nuclear Energy for New Europe 2008*, Portorož, Slovenia, September 8-11 (2008)
10. L. Mathieu et al., The thorium molten salt reactor: Moving on from the MSBR, *Progress in Nuclear Energy*, **48**, 664-679 (2006)
11. R.W. Moir, Recommendations for a restart of molten salt reactor development, *Energy Conversion and Management*, **49**, 1849-1858 (2008)
12. J. Křepel, U. Grundmann, U. Rohde, F.P. Weiss, DYN1D-MSR Dynamics Code for Molten Salt Reactors, *Annals of Nuclear Energy*, **32**, 1799-1824 (2005)
13. COMSOL Multiphysics®, User's Guide, version 3.4, COMSOL AB. (2007)
14. P. Mandin, H. Belachgar, A. Nuttin, G. Picard, Hydrothermal Modelling for the Molten Salt Reactor Design Optimisation, *Proceedings of NURETH-11*, Paper 227, Avignon, France, October 2-6 (2005)
15. I. Michiyoshi, Y. Kikuchi and O. Furukawa, Heat Transfer in a Fluid with Internal Heat Generation Flowing through a Vertical Tube, *Journal of Nuclear Science and Technology*, **5**, 590-595 (1968)

7. Appendix A. Nomenclature

A = interface heat transfer surface [m^2]
c = precursors concentration [m^{-3}]
$C_{P,f}$ = specific heat capacity of fluid [$J \cdot kg^{-1} \cdot K^{-1}$]
$C_{P,g}$ = specific heat capacity of graphite [$J \cdot kg^{-1} \cdot K^{-1}$]
$C_{\varepsilon 1}$ = k-ε model constant [-]
$C_{\varepsilon 2}$ = k-ε model constant [-]
C_{μ} = k-ε model constant [-]
D_c = precursors diffusion coefficient [$m^2 \cdot s^{-1}$]
D_n = neutron diffusion coefficient [m]
$F_{\perp}$ = horizontal component of volume force [$N \cdot m^{-3}$]
$F_{//}$ = vertical component of volume force [$N \cdot m^{-3}$]
g = gravity acceleration [$m \cdot s^{-2}$]
h = heat transfer coefficient [$W \cdot m^{-2} \cdot K^{-1}$]
I = identity matrix (2x2) [-]
k = turbulent kinetic energy [$m^2 \cdot s^{-2}$]
k_f = thermal conductivity of fluid [$W \cdot m^{-1} \cdot K^{-1}$]
k_g = thermal conductivity of graphite [$W \cdot m^{-1} \cdot K^{-1}$]
k_T = turbulent thermal conductivity [$W \cdot m^{-1} \cdot K^{-1}$]
m_g = mass of graphite [kg]
n = neutrons [-]
p = pressure of fluid [Pa]
Pr_T = turbulent Prandtl number [-]
S = amplitude of external neutron source [$n \cdot m^{-3} \cdot s^{-1}$]
S_g = energy source term within graphite [$W \cdot m^{-3}$]
S_n = external neutron source [$n \cdot m^{-3} \cdot s^{-1}$]
t = time [s]
T_0 = reference temperature [K]
T_f = temperature of fluid [K]
T_g = temperature of graphite [K]
u = velocity vector [$m \cdot s^{-1}$]
v_n = average velocity of neutrons [$m \cdot s^{-1}$]
α = coefficient of volume thermal expansion [K^{-1}]
β = fraction of neutrons emitted by precursors [-]
ε = turbulent dissipation rate [$m^2 \cdot s^{-3}$]
ε_f = heat produced per fission reaction [J]
η = dynamic viscosity of fluid [Pa·s]
η_T = eddy viscosity [Pa·s]
λ = decay constant of precursors [s^{-1}]
ν = average number of neutrons per fission [-]
ρ = density of fluid [$kg \cdot m^{-3}$]
ρ_0 = reference density of fluid [$kg \cdot m^{-3}$]
ρ_g = density of graphite [$kg \cdot m^{-3}$]
σ_k = k-ε model constant [-]
σ_{ε} = k-ε model constant [-]
Σ_a = absorption macroscopic cross section [m^{-1}]
Σ_f = fission macroscopic cross section [m^{-1}]
τ_g = time constant of graphite [s]
ϕ = neutron flux [$n \cdot m^{-2} \cdot s^{-1}$].

8. Appendix B. Governing equations

Fluid motion

$$\rho\frac{\partial u}{\partial t}+\rho u\cdot\nabla u=F+\nabla\cdot\left[-pI-\frac{2}{3}\rho kI\right]+ \\ +\nabla\cdot\left[\left(\eta+\eta_T\right)\left(\nabla u+(\nabla u)^T-\frac{2}{3}(\nabla\cdot u)I\right)\right] \quad (1)$$

$$\partial\rho/\partial t+\nabla\cdot(\rho u)=0 \quad (2)$$

$$\rho\frac{\partial k}{\partial t}+\rho u\cdot\nabla k=\nabla\cdot\left[\left(\eta+\frac{\eta_T}{\sigma_k}\right)\nabla k\right]-\rho\varepsilon+ \\ +\eta_T\left[\frac{1}{2}\left(\nabla u+(\nabla u)^T\right)^2-\frac{2}{3}(\nabla\cdot u)^2\right]-\frac{2}{3}\rho k\nabla\cdot u \quad (3)$$

$$\rho\frac{\partial\varepsilon}{\partial t}+\rho u\cdot\nabla\varepsilon=\nabla\cdot\left[\left(\eta+\frac{\eta_T}{\sigma_\varepsilon}\right)\nabla\varepsilon\right]-\rho C_{\varepsilon 2}\frac{\varepsilon^2}{k}+ \\ +C_{\varepsilon 1}\frac{\varepsilon}{k}\left\{\eta_T\left[\frac{1}{2}\left(\nabla u+(\nabla u)^T\right)^2-\frac{2}{3}(\nabla\cdot u)^2\right]-\frac{2}{3}\rho k\nabla\cdot u\right\} \quad (4)$$

Energy balance

$$\rho C_{P,f}\frac{\partial T_f}{\partial t}-\nabla\cdot\left[\left(k_f+k_T\right)\nabla T_f\right]= \\ S_f-\rho C_{P,f}u\cdot\nabla T_f \quad (5)$$

$$\rho_g C_{P,g}\frac{\partial T_g}{\partial t}+\nabla\cdot\left(-k_g\nabla T_g\right)=S_g \quad (6)$$

Neutron and precursors balance

$$\frac{1}{v_n}\frac{\partial\phi}{\partial t}=D_n\nabla^2\phi-\Sigma_a\phi+(1-\beta)\nu\Sigma_f\phi+\lambda c+S_n \quad (7)$$

$$\frac{\partial c}{\partial t}-D_c\nabla^2 c=\beta\nu\Sigma_f\phi-\lambda c-u\cdot\nabla c \quad (8)$$

Further expressions

$$F_\perp=0 \quad (i)$$

$$F_{//}=-g\alpha\rho_0\left(T_f-T_0\right) \quad (ii)$$

$$\rho=\rho_0\left(1-\alpha\left(T_f-T_0\right)\right) \quad (iii)$$

$$\eta_T=\rho C_\mu k^2/\varepsilon \quad (iv)$$

$$k_T=C_{P,f}\eta_T/Pr_T \quad (v)$$

$$S_f=\nu\Sigma_f\varepsilon_f\phi \quad (vi)$$

$$\tau_g=C_{P,g}m_g/(hA) \quad (vii)$$

9. Appendix C. Reference data

Table 1: Material properties and constants

Physical quantity	Value	Unit
$C_{P,f}$	1983	$J\cdot kg^{-1}\cdot K^{-1}$
$C_{P,g}$	1760	$J\cdot kg^{-1}\cdot K^{-1}$
$C_{\varepsilon 1}$	1.44	-
$C_{\varepsilon 2}$	1.92	-
C_μ	0.09	-
D_n	0.05	m
g	9.80	$m\cdot s^{-2}$
k_f	0.45	$W\cdot m^{-1}\cdot K^{-1}$
k_g	31.2	$W\cdot m^{-1}\cdot K^{-1}$
Pr_T	0.85	-
S	$1.4\cdot10^{15}$	$n\cdot m^{-3}\cdot s^{-1}$
S_g	$4.7\cdot10^{3}$	$W\cdot m^{-3}$
T_0	830	K
v_n	2200	$m\cdot s^{-1}$
α	$3.5\cdot10^{-4}$	K^{-1}
β	$6.0\cdot10^{-3}$	-
ε_f	$3.2\cdot10^{-11}$	J
η	$2.0\cdot10^{-3}$	Pa·s
λ	0.3	s^{-1}
$\nu\cdot\Sigma_f$	1.96	m^{-1}
ρ_0	2000	$kg\cdot m^{-3}$
ρ_g	1843	$kg\cdot m^{-3}$
σ_k	1.0	-
σ_ε	1.3	-
Σ_a	1	m^{-1}